Translational Science

Cancer Research

Zika Virus Selectively Kills Aggressive Human Embryonal CNS Tumor Cells *In Vitro* and *In Vivo*

Carolini Kaid[1], Ernesto Goulart[1], Luiz C. Caires-Júnior[1], Bruno H.S. Araujo[2], Alessandra Soares-Schanoski[3], Heloisa M.S. Bueno[1], Kayque A. Telles-Silva[1], Renato M. Astray[3], Amanda F. Assoni[1], Antônio F.R. Júnior[1], Daniella C. Ventini[3], Ana L.P. Puglia[3], Roselane P. Gomes[3], Mayana Zatz[1], and Oswaldo K. Okamoto[1]

Abstract

Zika virus (ZIKV) is largely known for causing brain abnormalities due to its ability to infect neural progenitor stem cells during early development. Here, we show that ZIKV is also capable of infecting and destroying stem-like cancer cells from aggressive human embryonal tumors of the central nervous system (CNS). When evaluating the oncolytic properties of Brazilian Zika virus strain ($ZIKV^{BR}$) against human breast, prostate, colorectal, and embryonal CNS tumor cell lines, we verified a selective infection of CNS tumor cells followed by massive tumor cell death. $ZIKV^{BR}$ was more efficient in destroying embryonal CNS tumorspheres than normal stem cell neurospheres. A single intracerebroventricular injection of $ZIKV^{BR}$ in BALB/c nude mice bearing orthotopic human embryonal CNS tumor xenografts resulted in a significantly longer survival, decreased tumor burden, fewer metastasis, and complete remission in some animals. Tumor cells closely resembling neural stem cells at the molecular level with activated Wnt signaling were more susceptible to the oncolytic effects of $ZIKV^{BR}$. Furthermore, modulation of Wnt signaling pathway significantly affected $ZIKV^{BR}$-induced tumor cell death and viral shedding. Altogether, these preclinical findings indicate that $ZIKV^{BR}$ could be an efficient agent to treat aggressive forms of embryonal CNS tumors and could provide mechanistic insights regarding its oncolytic effects.

Significance: Brazilian Zika virus strain kills aggressive metastatic forms of human CNS tumors and could be a potential oncolytic agent for cancer therapy. *Cancer Res; 78(12); 3363–74.* ©*2018 AACR.*

Introduction

The recent outbreak of Zika virus (ZIKV), especially throughout South and Central Americas, revealed an unprecedented impact of gestational infection on neurodevelopment, resulting in severe central nervous system (CNS) development effects in neonates, such as microcephaly and other associated abnormalities (1). Recent studies showed that ZIKV prominently infects neural stem and progenitor cells (NPC) and disrupts key cellular processes, e.g., survival, proliferation, and differentiation (2, 3), leading to massive cell death and growth reduction.

Notably, aggressive CNS embryonal tumors with high incidence in infants are originated from NPC aberrations, affecting key cell signaling pathways that regulate neurogenesis, such as the mTOR/Wnt pathway (4). These tumors are comprised by cells with neural stem–like features, also known as cancer stem cells (CSC), which are highly tumorigenic and resistant to classical cancer therapies (5). CNS tumors enriched in stem-like cancer cells are very difficult to treat and usually associated with poor prognosis (6). Available therapies have a low efficiency and severe adverse effects that include endocrine, motor, and cognitive deficits.

Oncolytic viral therapy has emerged as an alternative approach to treat aggressive, fast-growing forms of cancer. Oncolytic viruses are defined as native or genetically modified viruses that are able to directly infect and lyse tumor cells (7). Because ZIKV infects preferentially NPC, we hypothesized that $ZIKV^{BR}$ could act as an oncolytic agent in particular against aggressive and metastatic human CNS embryonal tumors.

Materials and Methods

Human and animal samples

The study followed the International Ethical Guideline for Biomedical Research (CIOMS/OMS, 1985) and was approved by the Institutional Animal Experimentation Ethics Committee (CEUA-USP 290/2017; CEUA-Instituto Butantan 3473210817). A total of 66 animals were included in the present study. Animals with 30% weight loss and/or visible tumor and/or ataxia and/or

[1]Human Genome and Stem Cell Research Center, Department of Genetics and Evolutionary Biology, Biosciences Institute, University of São Paulo (USP), São Paulo, Brazil. [2]Brazilian Biosciences National Laboratory (LNBio), Brazilian Center for Research in Energy and Materials (CNPEM), Campinas, São Paulo, Brazil. [3]Butantan Institute, São Paulo, Brazil.

Note: Supplementary data for this article are available at Cancer Research Online (http://cancerres.aacrjournals.org/).

C. Kaid, E. Goulart, and L.C. Caires-Júnior contributed equally to this article.

M. Zatz and O.K. Okamoto are senior authors of this article.

O.K. Okamoto is the lead contact of this article.

Corresponding Authors: Oswaldo K. Okamoto, University of São Paulo, São Paulo, SP 05508-900, Brazil. Phone: 55-11-30488357; E-mail: keith.okamoto@usp.br; and Mayana Zatz, Phone: 55-11-30910850; E-mail: mayazatz@usp.br

doi: 10.1158/0008-5472.CAN-17-3201

freezing were subjected to euthanasia, and all efforts were made to minimize suffering. Human samples (peripheral blood and tumors) were obtained after written informed consent of the patients, according to protocol approved by the Internal Review Board (CEP-IB No. 121/2011).

Cell lines and cultures

Three embryonal CNS tumor cell lines: DAOY (medulloblastoma, ATCC HTB-186), USP13-MED (medulloblastoma, in-house established; ref. 8), and USP7-ATRT (atypical teratoid/rhabdoid tumor, in-house established); three non-CNS tumor cell lines: MCF-7 (breast cancer, ATCC HTB-22), HCT-8 (colorectal cancer, ATCC CCL-244), and DU-145 (prostate cancer, derived from brain metastasis, ATCC HTB-81); one control human-induced pluripotent stem cell (hiPSC, C2535, in-house reprogrammed)–derived NPCs and neurons were analyzed. Detailed information regarding the generation and characterization of hiPSCs, NPCs, and neurons is provided in Supplementary Materials. All commercial tumor cell lines were grown according to ATCC recommendations, and cell authentication was performed by high-resolution karyotype analysis. USP13-MED and USP7-ATRT were isolated and characterized as previously reported (8). After thawing, all cell lines were cultured under standard conditions (5% CO_2 (g) at 37°C) up to 4 weeks (passages 1–4) and tested for *Mycoplasma* contamination by PCR (Cat. MP002; Sigma-Aldrich), before use in the described experiments.

Zika virus strain

$ZIKV^{BR}$ was donated by Dr. Pedro Vasconcelos, Instituto Evandro Chagas, Brazil. Viral stock was established in VERO cells, cultured in serum-free medium (VP-SFM, Thermo Scientific) after two serial passages at a multiplicity of infection (MOI) of 0.05, and supernatants harvested after 72 hours. Virus stocks were titrated by plaque-forming units (PFU) assay on VERO cells.

In vitro two-dimensional and three-dimensional infection with $ZIKV^{BR}$

Cells (4.2×10^3 cells/cm^2) in two-dimensional were exposed to $ZIKV^{BR}$ (MOI: 0.01, 0.1, 1, and 2) or Mock for 1 hour at 37°C, washed with culture medium, and maintained up to 72 hours. Tumorspheres (three-dimensional, 3D), generated and characterized as previously reported (8), were infected with MOI 1, 2, or Mock, with viral exposure for 2 hours to ensure complete sphere infection. $ZIKV^{BR}$ PFU and copy numbers were analyzed from supernatant media every 24 hours. Total viable cells and spheres area were daily evaluated with ImageJ software.

Functional $ZIKV^{BR}$ yielding analysis

Tumor cells were infected with $ZIKV^{BR}$ (MOI 1), based on prior PFU results of all tested cell lines. Seventy-two hours later, culture supernatants were harvested and used to infect human NPC (8.4×10^4 cells/cm^2 infected with 1.26×10^6 $ZIKV^{BR}$ viral copies). After another 72 hours, NPC culture supernatants were harvested for PFU analysis in order to verify the efficiency of functional $ZIKV^{BR}$ yielding by each tumor cell line. The volumes used to infect NPC were calculated based on qRT-PCR results.

Immunofluorescence

Brain sections and fixed tumor cells (3.7% formaldehyde for 10 minutes) were treated for 30 minutes with 0.1% Triton X-100 in 1× PBS, prior to 2-hour incubation in 5% bovine serum albumin in 1× PBS, and then incubated overnight with the primary antibody (Supplementary Table S1) at 4°C. Brain sections and cells were then washed 3 times in 1× PBS, incubated with the secondary antibody for 2 hours (Supplementary Table S1), and washed again 2 times in 1× PBS. Cell nuclei were stained with 1 μg/mL DAPI for 2 minutes. Tissue sections and tumor cells were mounted on glass slides and cover slipped with VectaShield. All images were taken in confocal microscope (Zeiss LSM 800).

Cell death analysis

Staining for caspase-3/7 (CellEvent, Thermo Fisher) and propidium iodide (PI) was performed in 1×10^5 tumor cells, 72 hours after infection with $ZIKV^{BR}$, following the manufacturer's protocol. Flow cytometry analysis was performed using FACS Aria II (BD) collecting 10,000 events per run. Analysis was carried using FlowJo software.

Wnt–β-catenin pathway modulation

Cell lines (USP7-ATRT, USP13-MED, and DAOY) were cultured as previously described, with addition of CHIR99021 (Wnt pathway inductor; 5 nmol/L, 50 nmol/L, 100 nmol/L, 500 nmol/L, or 1,000 nmol/L), IWP-2 (Wnt pathway inhibitor; 20 nmol/L, 100 nmol/L, 200 nmol/L, 1,000 nmol/L, or 2,000 nmol/L), or DMSO (dilution reagent for CHIR99021 and IWP-2), together with $ZIKV^{BR}$ (MOI 0.1). Seventy-two hours after viral infection, β-catenin expression (see Supplementary Table S1), cell death, and virus titration were evaluated.

Orthotopic metastatic xenograft model/$ZIKV^{BR}$ *in vivo* injection assay

Tumor cells expressing firefly luciferase were generated with pLV/Luc lentiviral vector, as previously described (9). The orthotopic metastatic model was performed as previously described in detail (10). After tumor establishment, according to cell line–dependent growth kinetics (Ti = 1 week for USP7-ATRT and 2 weeks for USP13-MED and DAOY), 2×10^3 $ZIKV^{BR}$ particles/2 μL were injected in the right lateral ventricle. Sham group was injected with DMEM, instead of tumor cells. The initial amount of animals per experimental group was 10. Few animals died during the surgery procedure and therefore could not be included in the experiment. Tumor development was assessed *in vivo* with IVIS Imaging System (PerkinElmer) as previously described (8). Metastasis classification followed M-Stage proposed by Chang's system (11). Tumor detection was confirmed by histologic and immunofluorescence analyses. Tumor remission in each experimental animal was evaluated by time course analysis of normalized bioluminescence levels (photon counts) and considered if respective bioluminescence levels in T1, T2, or T3/Ti < 1. Animal activity was monitored as described in Supplementary Materials.

Molecular analysis

Gene expression profiling was determined with Affymetrix GeneChip Human Gene 2.0 ST whole-transcript arrays (GEO accession number: GSE103935). Identification (12) and interactome analysis of differentially expressed genes were performed

with Transcriptome Analysis Console (Affymetrix) and IPA Software (Ingenuity Pathway Analysis, Qiagen), respectively. Whole-exome sequencing was performed using Illumina's TrueSeq kits and the Illumina HiSeq sequencer. Candidate pathogenic mutations were determined by allele frequency < 0.05 in NIH 1000 Genomes Project and by SIFT and FATHMM algorithms. Array comparative genomic hybridization was performed using 60K whole-genome platform (Agilent Technologies) following the manufacturer's recommendation. Detailed description is provided in Supplementary Experimental Procedures.

Statistical analysis

All experiments were performed in triplicate, and three independent experiments were carried out. Data were analyzed by one-way and two-way ANOVA followed by Bonferroni *post hoc* test. The *t* test with two-tailed unpaired test was used for pairwise comparison. Clinical and pathologic parameters were analyzed by the Fisher exact test. Graphpad Prism software was used to perform all statistical analysis (version 6.0 GraphPad Software Inc.). Quantification of data is represented as mean ± SEM, and *P* value threshold was as follows: *, 0.05; **, 0.01; ***, 0.001; and ****, 0.0001.

Results

Oncolytic *in vitro* effects of ZIKV^{BR}

In order to evaluate ZIKV^{BR} oncolytic properties in different tumors, six human tumor cell lines were tested against various MOIs: 0.01, 0.1, 1, and 2. Three non-CNS cell lines, MCF-7, HCT-8, and DU-145, and three CNS embryonal tumor cell lines, USP13-MED (7), DAOY, and USP7-ATRT, were infected in monolayer cultures. Figure 1 and Supplementary Fig. S1A show that 72 hours postinfection (hpi), ZIKV^{BR} induced significant cell death and/or growth reduction in DAOY, USP13-MED, and more pronounced death in USP7-ATRT, starting at MOI 0.1. At least 50% of the USP7-ATRT and USP13-MED cell populations were already infected starting at MOI 0.1 at 48 hpi. Under the same conditions, infection of DAOY cells was less effective, reaching a maximum of about 40% of infected cells at MOI 1 and 2.

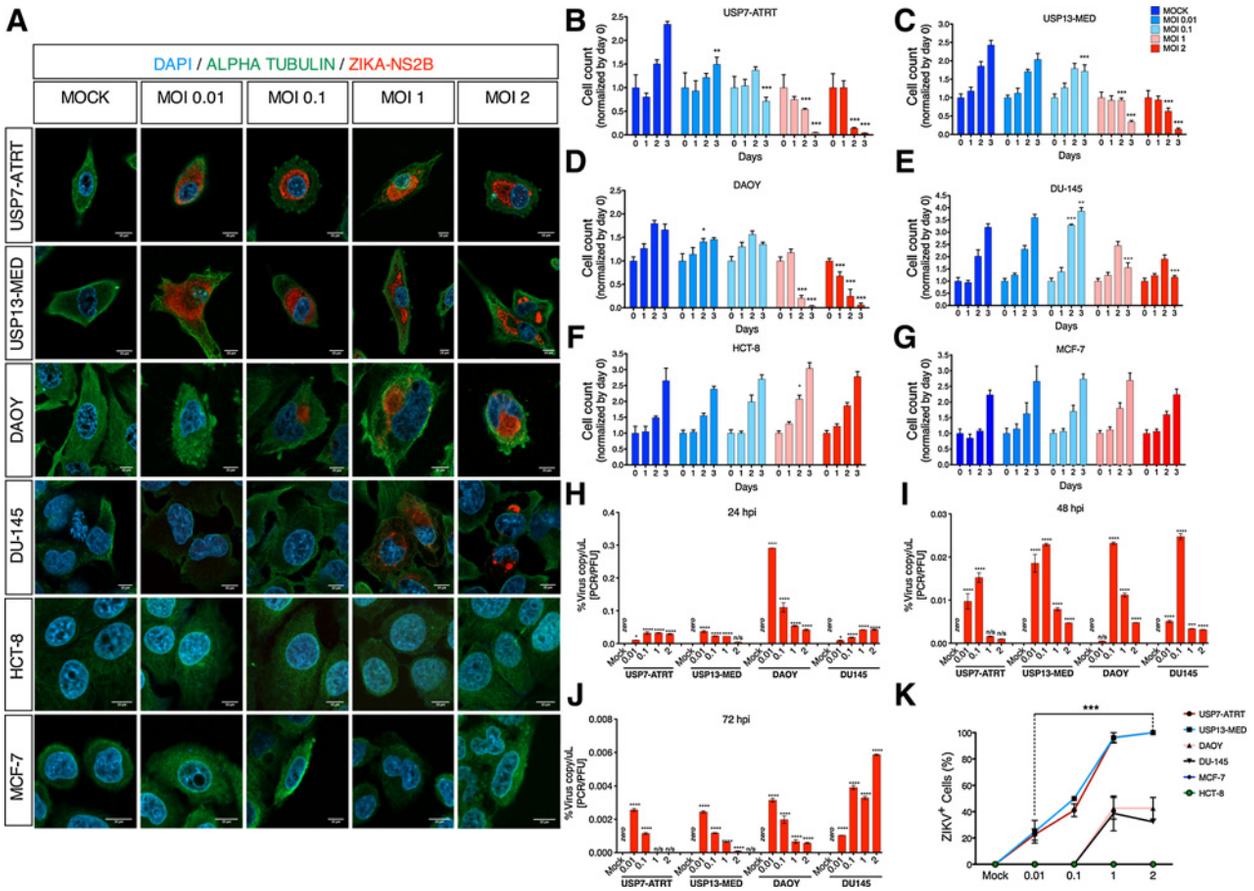

Figure 1.

Oncolytic effects of ZIKV^{BR} against CNS and non-CNS tumor cells *in vitro*. **A,** Immunofluorescence staining of ZIKV^{BR} in all conditions and cell lines at 48 hpi. Scale bar, 10 μm. **B–G,** Total cell number of CNS and non-CNS tumor cell lines infected by ZIKV^{BR} at different MOI conditions at 24, 48, and 72 hpi (*, $P < 0.05$; **, $P < 0.01$; and ***, $P < 0.001$, two-way ANOVA compared with respective day mock condition; $n = 5$ replicates per cell line). **H–J,** Percentage of PFU relative to total viral RNA copies on culture supernatants at 24, 48, and 72 hpi, respectively (****, $P < 0.0001$, two-way ANOVA always compared with respective day mock condition; $n = 3$ replicates per cell line). **K,** Percentage of ZIKV^{BR}-positive stained cells of all tumor lines and conditions at 48 hpi (***, $P < 0.001$, two-way ANOVA; $n = 3$ replicate per cell line). See also Supplementary Fig. S1.

Complementary flow cytometry analysis (Fig. 2A and B) showed that ZIKV^{BR} infection significantly increased the population of PI-positive cells, whereas caspase-3/7–positive cells remained low in all CNS tumor cell lines. Confocal microscopy analysis confirmed the presence of ZIKV^{BR} particles within the cytoplasm (Fig. 2C). On the other hand, exposure to ZIKV^{BR} had little or no effect on

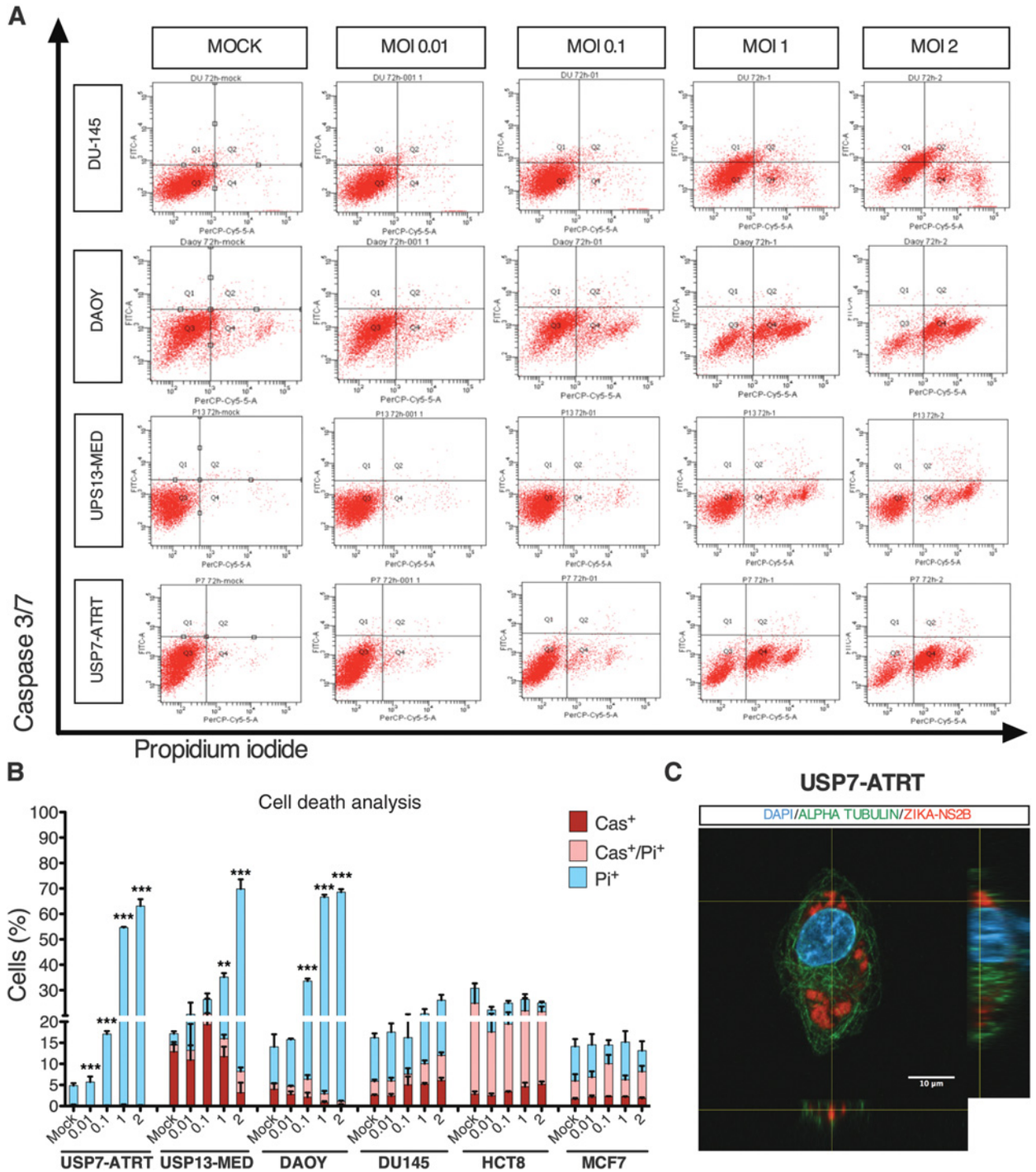

Figure 2.

ZIKV^{BR} induces cell death *in vitro* involving rupture of the plasma membrane. **A,** Flow cytometry gating and acquired events in USP7-ATRT, USP13-MED, DAOY, and DU-145 cells stained for PI and caspase at 72 hpi ($n = 3$ replicate per cell line). **B,** Flow cytometry staining analysis of PI and caspase-3/7 (Cas; *, $P < 0.05$; **, $P < 0.01$; and ***, $P < 0.001$, two-way ANOVA always compared with respective mock condition; $n = 3$ replicates per cell line). **C,** Orthogonal view of USP7-ATRT ZIKV^{BR} staining.

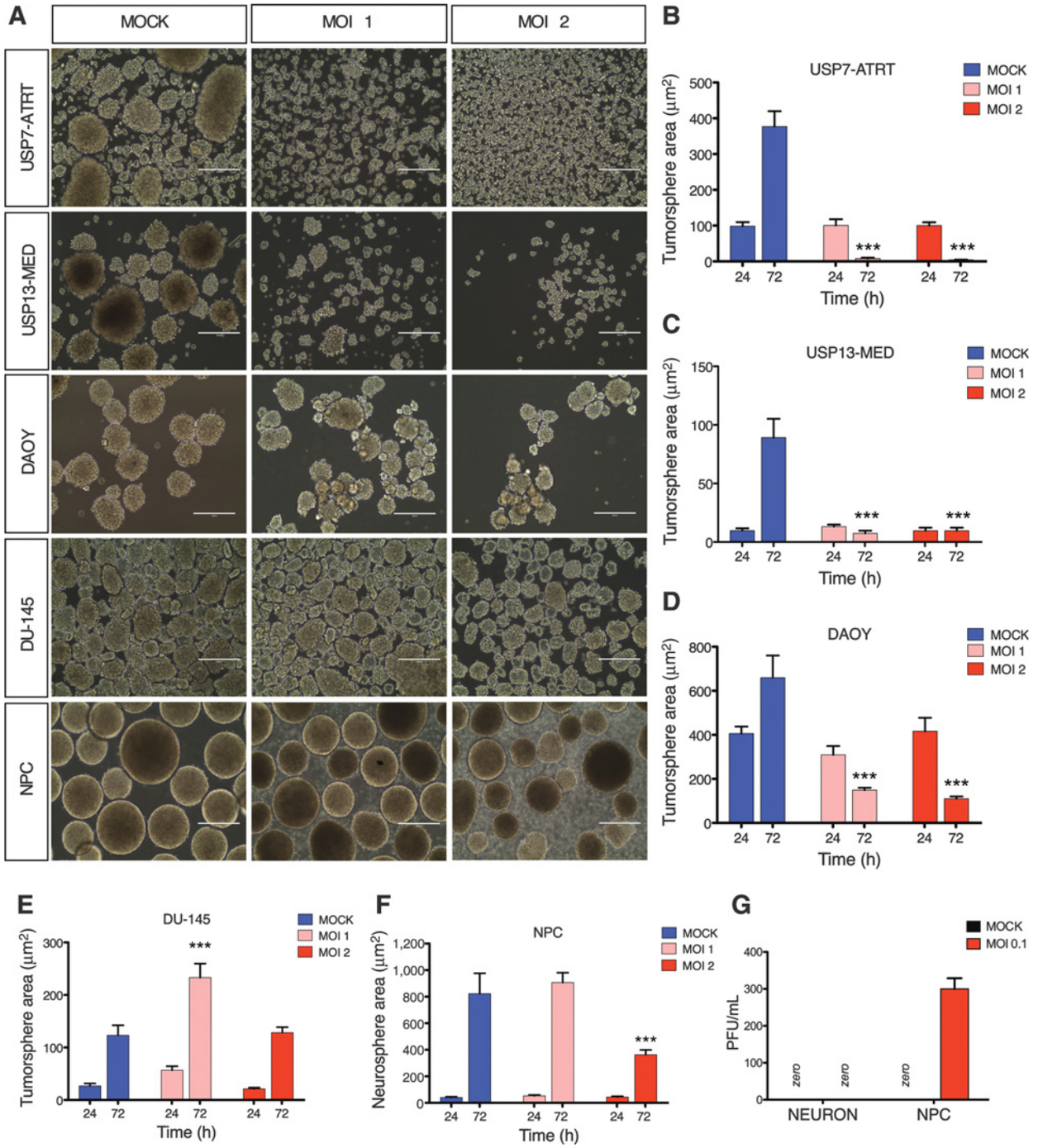

Figure 3.

Oncolytic effects of ZIKV^{BR} in tumorspheres and normal neurospheres. **A,** Representative phase contrast images of tumorspheres and neurospheres at 72 hpi. Scale bar, 400 µm. **B–F,** Area quantification of USP7-ATRT, USP13-MED, DAOY, DU-145 tumorspheres, and normal hiPSC-derived NPC neurospheres after 24 and 72 hours of ZIKV^{BR} infection (*, $P < 0.05$; **, $P < 0.01$; and ***, $P < 0.001$, two-way ANOVA always compared with respective mock condition; $n = 30$ tumorsphere per cell line). Scale bar, 400 µm. **G,** PFU on culture supernatant 48 hours after normal hiPSC-derived NPC and neuron ZIKV^{BR} infection (MOCK and MOI 0.1).

non-CNS tumor cell lines. These results indicate that ZIKV^{BR} induces death involving rupture of the plasma membrane of CNS embryonal tumor cells.

Interestingly, viral titer quantification showed that all CNS embryonal tumor cells produced high amounts of infectious viral particles starting at 24 hpi, but, after 72 hpi, these cells

started producing defective viral particles, indicative of host cell dysfunction (Supplementary Fig. S1B–S1D). MCF-7 and HCT-8 cells did not produce significant amounts of ZIKV^{BR} (Supplementary Fig. S1E). Of note, DU-145 cells showed high viral titers during all the infection kinetics experiment, which supports ZIKV^{BR} clinical findings of prolonged viral titers found in human semen samples (13).

ZIKV^{BR} oncolytic effects in tumorspheres and normal neurospheres

All tumor cell lines susceptible to ZIKV^{BR} infection were then cultured in a CSC-tumorsphere promoting system and tested in parallel with normal hiPSC-derived NPC. Figure 3A–F shows that ZIKV^{BR} significantly disrupted CNS tumorspheres and produced high viral titers, particularly in USP7-ATRT cultures. Conversely, despite infected by ZIKV^{BR}, DU-145 tumorspheres were not disrupted, reinforcing a selective oncolytic effect toward the CNS tumor cells. Compared with the cell cultures in monolayer, the 3D culture system showed a greater impact of ZIKV^{BR} on cellular viability. Interestingly, normal NPC neurospheres were less affected by ZIKV^{BR} as compared with CNS embryonal tumorspheres. Neurons derived from these normal NPC, however, were not infected by ZIKV^{BR} (Fig. 3G). Of note, single cells from dissociated CNS embryonal tumorspheres were not capable of forming new tumorspheres after ZIKV infection (Supplementary Fig. S1F and S1G). For characterization of hiPSC, NPC, and neurons, see Supplementary Fig. S2. Together, these results suggest that proliferative tumor cells from CNS origin are more permissive to ZIKV^{BR} infection and virus-mediated death than normal nervous system cells and tumors from other primary origins such as breast, colorectal, and prostate.

ZIKV^{BR} effects in tumor development and metastasis

Next, we tested ZIKV^{BR} oncolytic properties in an orthotopic xenograft animal model in BALB/c nude mice with DAOY, USP13-MED, and USP7-ATRT cell lines. A single dose of 2×10^3 infectious viral particles was injected in the right ventriculum after respective tumor engraftment period of DAOY, USP13-MED, and USP7-ATRT cell lines (Fig. 4A).

After few weeks of viral particles administration, striking results were observed. ZIKV^{BR} induced tumor remission in 20 of 29 animals (USP7-ATRT: 8/10; USP13-MED: 8/9; DAOY: 4/10; Supplementary Fig. S3A–S3C), 7 of which achieved complete remission (two USP7-ATRT and six USP13-MED). Of note, an additional USP7-ATRT–bearing mice had complete remission 3 weeks after ZIKV^{BR} injection, but it was not included in our analysis due to lack of imaging acquisition at the time of injection (Ti). Overall survival of USP7-ATRT tumor–bearing mice was significantly improved ($P = 0.0046$) by ZIKV^{BR} treatment (Fig. 4B). Three cases of tumor relapse after complete remission were observed in ZIKV^{BR}-treated animals with USP13-MED tumors. Figure 4C–G shows a marked reduction of USP7-ATRT and USP13-MED tumor growth ratio, whereas a poor response of DAOY tumors to ZIKV^{BR} was detected *in vivo*, which is consistent with the relative lower rates of cell infection previously observed for this cell line.

In addition, in ZIKV^{BR}-treated animals, 60% (3 of 5) of USP7-ATRT tumor–bearing mice had complete metastatic remission, and none of the USP13-MED tumor–bearing mice developed M3 metastasis (Table 1). USP7-ATRT and USP13-MED cell lines were the only capable of generating M3 stage metastasis (tumors in the spinal cord), which occurred in 66% (6 of 9) and 33% (3 of 9) of animals from the mock group, respectively (Table 1).

USP7-ATRT cells formed the most aggressive tumors in our experimental model, being the only tumor cell line causing 100% of death rate in the mock control group within 30 days of experimental follow-up. The same poor survival was observed in mice orthotopically injected in low density of cell (2×10^5 per animal). The AT/RT cell line was able to generate M2 and M3 metastatic tumors after 1 week (Supplementary Fig. S4A–S4G).

Histologic analysis confirmed necrotic tumor foci and ZIKV^{BR}-positive tumor cells in brain tissue of USP7-ATRT and USP13-MED tumor–bearing mice (Supplementary Fig. S5A), but significant improvement in overall survival was detected only for animals bearing USP7-ATRT tumors (Supplementary Fig. S5B and S5C). In tumor-bearing mice, viral titer in brain, spinal cord, peripheral blood, and spleen indicated that ZIKV^{BR} infection was more consistently persistent and restricted to host CNS at the time of euthanasia. Interestingly, sham animals (without tumor cell injection) that were only infected with ZIKV^{BR} had persistent virus in peripheral blood, brain, spinal cord, and spleen and decreased survival rate as compared with those bearing tumors (Supplementary Fig. S5D–S5G). These results are in agreement with the previous observation of high noninfectious viral particle production by host tumor cells, especially in USP7-ATRT. The ZIKV^{BR}-mediated cell lysis in USP7-ATRT is so intense that it rapidly destroys tumor sites hampering viral infection amplification.

NPC-like tumor cells are more prone to ZIKV^{BR}-mediated oncolysis

Among the tumor cell lines tested, USP7-ATRT and USP13-MED displayed the highest levels of viral infection, USP7-ATRT being the most sensitive to ZIKV^{BR}-mediated oncolysis. USP7-ATRT cells are highly invasive and proliferative, with a population doubling time (PDT) of 24.16 hours (Supplementary Fig. S6A–S6C). However, the higher USP7-ATRT sensitivity to ZIKV^{BR} is unlikely related to cell proliferation rates because its PDT is equivalent to those from USP13-MED (24.5 hours) and DAOY (29.8 hours) cells (8). Also, both USP7-ATRT and USP13-MED (8) cell lines are enriched in highly tumorigenic CSC with increased resistance to chemotherapeutic agents and capability of generating tumorspheres (Supplementary Fig. S6D–S6H).

A more detailed analysis, integrating whole-exome sequencing, chromosomal copy-number aberrations, and global gene expression profiling, revealed TP53, CDKN1A, CTNNB1, and CCND1 as hotspots of an interactome map of affected proteins in USP7-ATRT cells (Fig. 5). Interestingly, the molecular profile of USP7-ATRT is consistent with SMARCB1/INI1-positive type of AT/RT (Supplementary Fig. S6I–S6O), known to be closely related to normal neural stem cells (14). In fact, USP7-ATRT cells express typical neural stem cell markers (Fig. 5A and B), and a comparative global gene expression profiling revealed a stronger similarity of USP7-ATRT cells with normal NPC than with other CNS embryonal tumors (Fig. 5C–F). In addition, USP7-ATRT cells and NPC are highly similar regarding the pattern of expression of TAM receptor genes and other genes associated with ZIKV^{BR} cellular entry (15, 16, 17). Such neural stem cell molecular fingerprint is correlated with a higher sensitivity of USP7-ATRT cells to ZIKV^{BR}-mediated oncolysis, as compared with the other tumor cell lines.

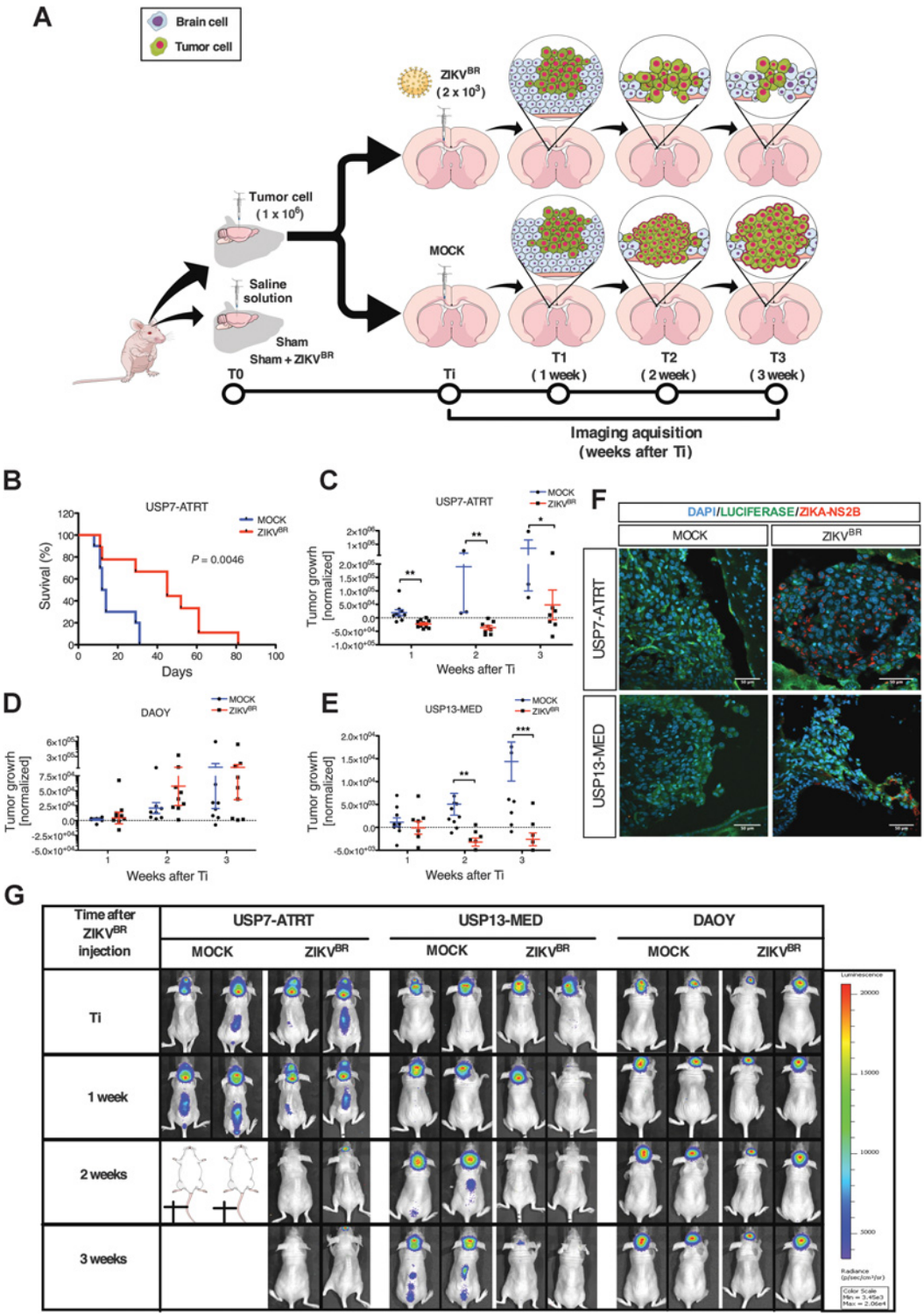

Figure 4.

Oncolytic effects of single intracerebroventricular ZIKV^{BR} administration in mice bearing orthotopic CNS embryonal tumor xenografts. **A,** Visual representation of the *in vivo* experimental layout. **B,** Overall survival rates of USP7-ATRT tumor–bearing mice (*, $P < 0.05$, log-rank Mantel–Cox test; $n = 10$ per ZIKV^{BR} group and n=9 per MOCK group). **C–E,** Bioluminescence-based analysis of USP7-ATRT, USP13-MED, and DAOY tumor development (*, $P < 0.05$; **, $P < 0.01$; and ***, $P < 0.001$, two-way ANOVA always compared with respective mock condition; $n = 10$ per ZIKV^{BR} group (red) and n=9 per MOCK group (blue). **F,** Representative images of brain tissue immunofluorescent staining for firefly luciferase–positive tumor cells and ZIKV^{BR} from tumor-bearing mice. See also Supplementary Fig. S5. **G,** Representative bioluminescence-based images of tumor development in control (mock) and ZIKV^{BR}-treated mice ($n = 10$ per ZIKV^{BR} group and n=9 per MOCK group). Scale bar, 50 μm.

Table 1. Clinical and pathologic parameters of BALB/c nude mice bearing orthotopic human embryonal CNS tumor cells and subjected to ZIKV^{BR} infection

Tumor	USP7-ATRT		USP13-MED		DAOY	
Ti	Mock	ZIKV^{BR}	Mock	ZIKV^{BR}	Mock	ZIKV^{BR}
Activity gain	0/4	2/4	1/4	0/4	3/4	3/4
Weight gain	1/9	7/10[a]	4/9	5/9	5/9	6/10
Weight loss	8/9[a]	4/10	6/9	4/9	2/9	7/10
Event M3	6/9	5/10	3/9	0/9	0/9	2/10
Tumor remission	0/9	8/10[b]	0/9	8/9[b]	0/9	4/10
Tumor relapse	—	2/8	—	4/9	—	4/4
M3 remission	0/7	3/5	0/3	—	—	—
M3 recover	—	0/3	—	—	—	—

NOTE: Events expressed in ratios of number of animals/group/Ti. Weight gain and weight loss correspond to 10% to 30% alteration based on the initial animal body weight along time. M3 corresponds to advanced stage of tumor metastasis in the neural axis according to Chang's staging system (11). Statistical analysis following the Fisher exact test.

[a] *, $P < 0.05$, statistical analysis following the Fisher exact test.

[b] ***, $P < 0.001$, statistical analysis following the Fisher exact test.

Wnt/β-catenin activity modulates ZIKV^{BR}-induced oncolysis and efficient viral replication in tumor cells

USP7-ATRT was the most sensitive cell line to the oncolytic properties of ZIKV^{BR}, and the comparative molecular analysis suggested that the Wnt pathway is hyperactive in this specific tumor cell line (Fig. 5G). Given the involvement of the Wnt pathway in normal neural development and tumorigenesis, we further investigated a possible role of Wnt/β-catenin signaling in ZIKV^{BR} susceptibility.

All CNS embryonal tumor cell lines were treated with CHIR99021 or IWP-2, an activator and an inhibitor of Wnt/β-catenin signaling, respectively. Both small molecules were not cytotoxic in mock-infected cells at the concentrations used in this study for all cell lines tested (Supplementary Fig. S7A and S7B). The CHIR99021 treatment significantly increased ZIKV^{BR}-mediated oncolysis of USP7-ATRT and USP13-MED cells, whereas IWP-2 treatment significantly attenuated such virus effect in USP7-ATRT (Fig. 6A and B; Supplementary Fig. S7C–S7F). Although unlikely, a possible cytotoxicity due to a synergistic effect of ZIKV^{BR} and CHIR99021 cannot be ruled out. ZIKV^{BR}-induced oncolysis was not affected by both treatments in DAOY cell line (Fig. 6C; Supplementary Fig. S7G and S7H). Western blotting analysis showed that CHIR99021 treatment efficiently modulated β-catenin expression in USP7-ATRT and USP13-MED, but not in DAOY (Fig. 6D and E). β-Catenin expression was altered by IWP-2 only in USP7-ATRT cell line. Basal β-catenin levels were significantly higher in USP7-ATRT compared with the other cell lines, confirming the previous global gene expression findings. CHIR99021 treatment also reduced efficient viral replication in USP7-ATRT cells (Fig. 6F).

Interestingly, production of infectious viral particles by host CNS tumor cells was not efficient. To address this question, USP7-ATRT, USP13-MED, and DAOY cells were first infected with MOI 1 ZIKV^{BR}, and 72 hours after tumor cell infection, respective supernatants of these cell cultures containing the same amount of ZIKV^{BR} copies were used to infect normal NPC at 72 hpi. In this cross-infection experiment, NPC infection with USP7-ATRT and USP13-MED supernatants did not produce functional ZIKV^{BR} particles, whereas infection with DAOY supernatant produced relatively few functional ZIKV^{BR} particles (Fig. 6G).

Discussion

Here, we compared six cell lines from five different human tumors (breast, prostate, colon rectal, and two different CNS embryonal tumors: ATRT and medulloblastoma), normal human NPC, and neurons. We show that ZIKV^{BR} oncolytic effects are not generalized to all kinds of cancer, but more specific to CNS tumors. Interestingly, we observed that ZIKV^{BR} kills CNS tumor cells more efficiently than normal NPC and that distinct CNS tumors may have differential sensitivity to ZIKV^{BR}, indicating a selective oncolytic property. Notably, ZIKV^{BR} injection improved overall survival, induced tumor remission, and effectively inhibited metastatic spread of human CNS tumor xenografts in athymic nude mice.

To our knowledge, this is the first study demonstrating oncolytic effects of ZIKV^{BR} against human tumor cells *in vivo*. A very recent study by Zhu and colleagues (18) reported that ZIKV can also infect and inhibit mouse glioblastoma in syngeneic mice, improving survival. However, it is known that animal models not always recapitulate human pathologies. Furthermore, these authors also showed that ZIKV can destroy human glioblastoma cells *in vitro*, but at a relatively high MOI of 5, for much longer periods of time (2–4 weeks), as compared with the lower 0.01–2 MOI range tested in our study up to 72 hours.

The demonstration of selective oncolytic effects at low infection rates is highly relevant regarding safety in possible clinical trials. Some studies reported prolonged viral shed in human CNS (19), but very few cases were reported in the literature as lethal ZIKV-associated infection (20). Postnatal, infant, and adult infection rarely results in clinically relevant findings [e.g., conjunctivitis (21), Guillain–Barré syndrome (22), and encephalitis (20)]. Nonetheless, most ZIKV-infected individuals remain asymptomatic (23), and, in general, prognosis of ZIKV infection is largely uneventful with few or no intervention required.

In our preclinical study, conjunctivitis, ataxia, inflammation, and behavior abnormalities were not detected in any of the experimental animal subjects. Interestingly, upon ZIKV^{BR} infection, overall survival of tumor-bearing mice was higher than that of sham animals. This higher mortality of control immunosuppressed mice raises an important safety issue and alert for possible adverse effects that cannot be ignored in future clinical development steps. Cross-infection experiments suggest that this effect may involve low production of functional viral particles by the infected tumor cells. The *in vitro* dose-escalation study at different time points also showed that infection with increasing virus MOI correlates with increasing tumor cell death and lower virus replication. This pattern was observed for the CNS tumor cell lines, with USP7-ATRT being the most affected cells. However, in this scenario, establishing optimal ZIKV

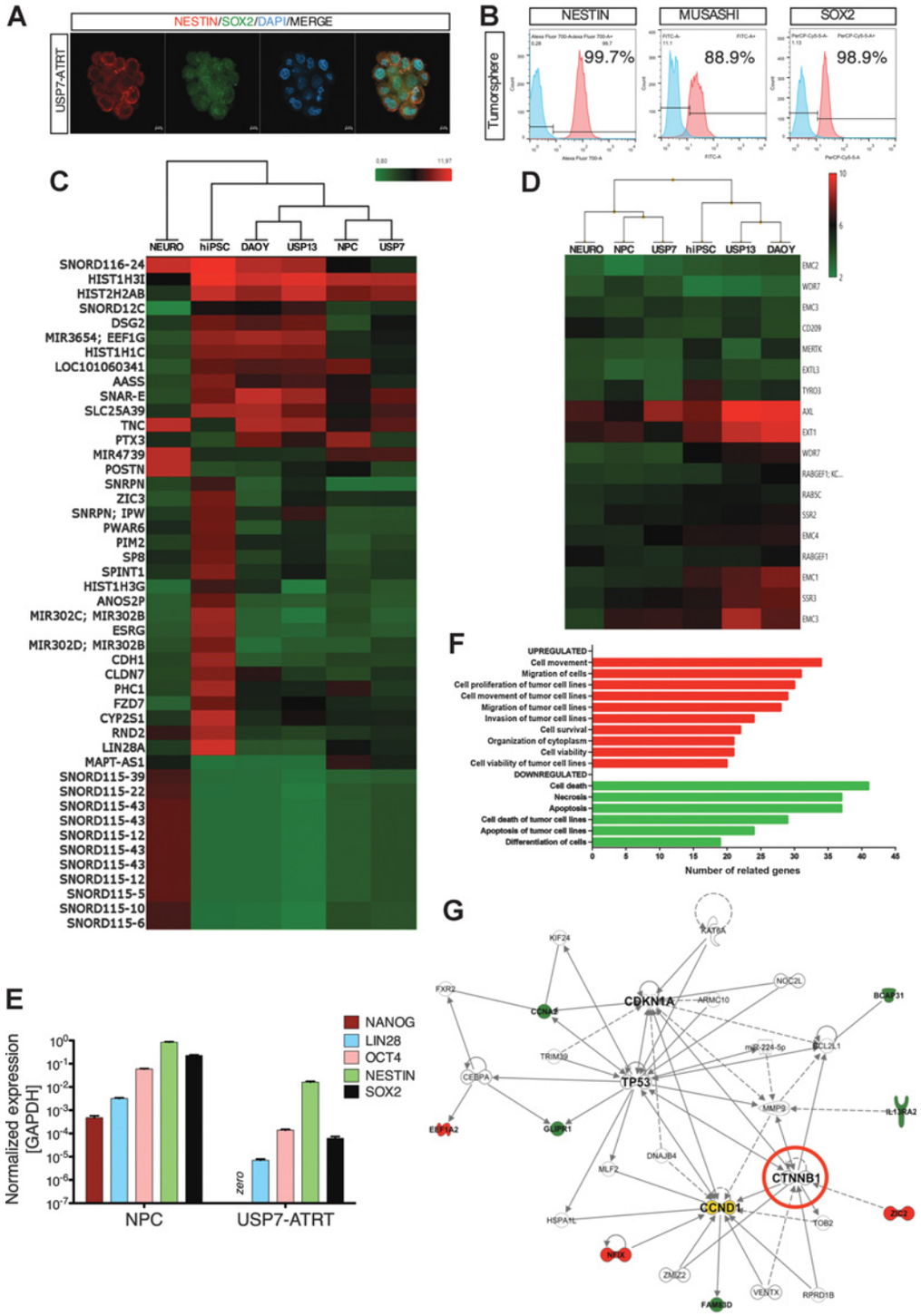

Figure 5.

USP7-ATRT gene profiling is more similar with NPC than with other CNS embryonal tumors. **A** and **B**, Nestin and SOX2 immunofluorescence staining and Nestin, SOX2, and Musashi-1 flow cytometry analysis of USP7-ATRT tumorspheres ($n = 3$ replicates). Scale bar, 5 μm. **C** and **D,** Cluster analysis of commonly differentiated expressed genes in all tumor cell lines prior to ZIKV^{BR} infection (**C**), and ZIKV^{BR} predict targets among noninfected embryonic CNS tumor cell lines and hiPSC and hiPSC-derived NPCs and neurons (**D**). Data are presented as average-normalized signal in $\log_2$ ($n = 2$ replicates per cell line). **E,** Expression profile of stem cell and neural stem cell markers in USP7-ATRT and hiPSC-derived NPCs by real-time PCR. **F,** Main functional categories and signaling pathways associated with upregulated or downregulated genes in USP7-ATRT cells relative to normal cerebellum. Genes were functionally classified according to Ensembl definition. **G,** Interactome mapping of proteins affected in USP7-ATRT cells, as indicated by an integrated analysis of global gene expression profiling prior to ZIKV^{BR}, chromosome copy-number aberration by array comparative genomic hybridization, and whole-exome sequencing data. See also Supplementary Figs. S2 and S6.

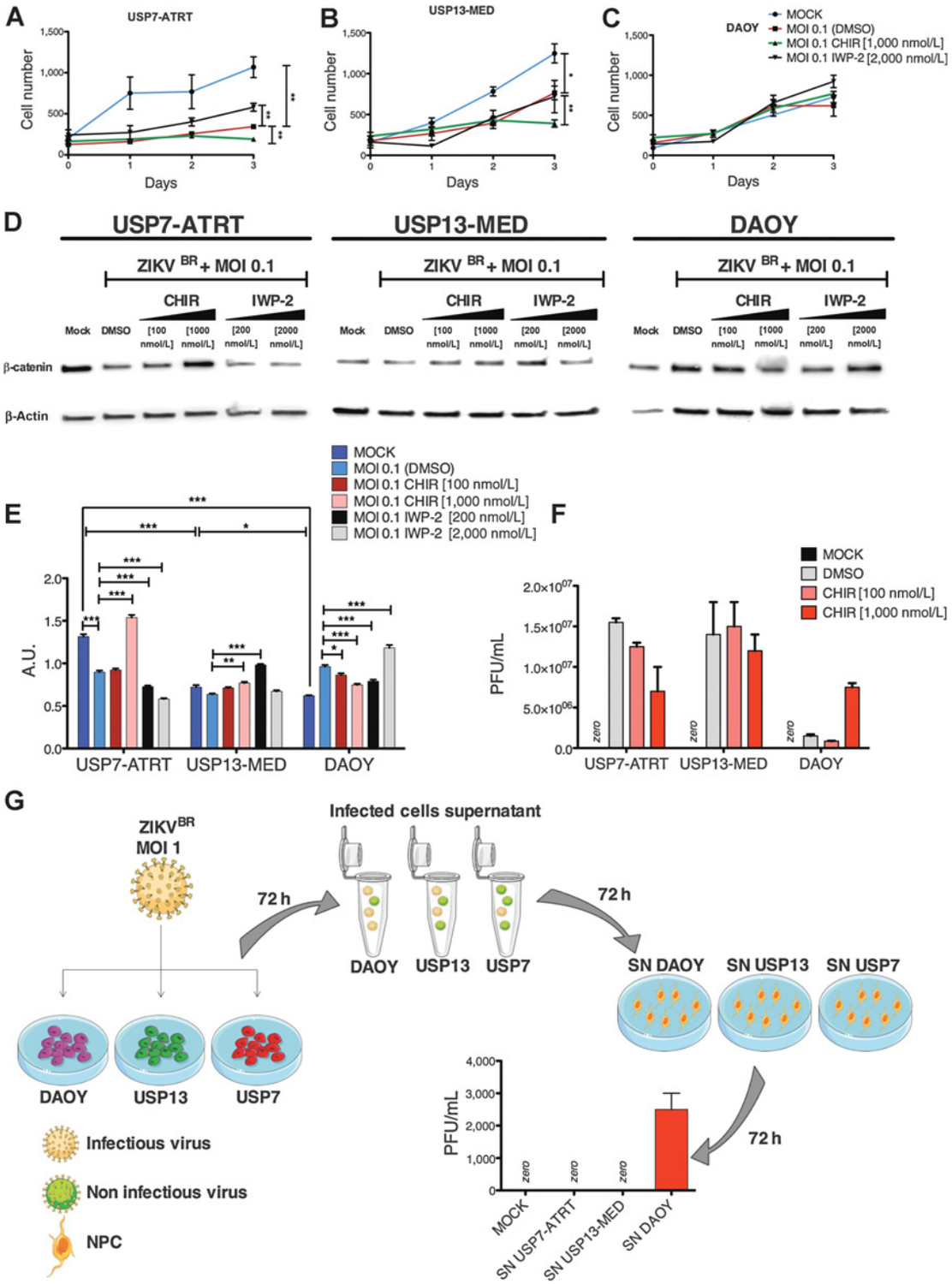

Figure 6.

ZIKV^{BR} oncolysis in response to Wnt/β-catenin activity modulation. **A–C**, Cell counting of ZIKV^{BR}-infected tumor cells (MOI = 0.1) treated with CHIR99021 or IWP-2 for 72 hours (*, $P < 0.05$; **, $P < 0.01$; and ***, $P < 0.001$, two-way ANOVA with Tukey multiple comparison test, nonlinear fit curve test; $n = 4$ per group). **D,** Western blotting of β-catenin of all tumor cell lines after 72 hpi and treated with CHIR99021 or IWP-2. **E,** β-Catenin Western blotting analysis (*, $P < 0.05$; **, $P < 0.01$; and ***, $P < 0.001$, one-way ANOVA with Dunnett multiple comparison test; $n = 3$ per group). **F,** PFU/mL of culture supernatant at 72 hpi and treated with CHIR99021 ($n = 2$, technical replicates). **G,** Schematic representation of tumor cell lines and NPC cross-infection experiment and result ($n = 2$, technical replicates).

dosing scheme required for efficient treatment of CNS tumors is paramount.

This lower virus replication in tumor cells can be explained by the fact that viruses use the host cell machinery to complete their replication. Thus, virus replication requires alive and fully functional host cells. In fact, death of host cells is a well-known defense mechanism that limits virus replication in infected cells, and some viruses encode cell death inhibitors to circumvent this defense and facilitate their own replication (24).

Among the CNS embryonal tumor cells lines, USP7-ATRT displayed the highest sensitivity to ZIKV^{BR}, which may be partly explained by the fact that ATRT is originated from early neural stem cells and neuroprogenitors (25), whereas medulloblastoma is thought to originate from more mature granular neurons and their progenitors (26). A closer molecular similarity of USP7-ATRT with NPC than with the other tumor cell lines was indeed confirmed by an integrated molecular study, which also highlighted CTNNB1 as a key affected protein in USP7-ATRT cells.

Unbalanced regulation of Wnt signaling effectors, like CTNNB1, is common in AT/RT (27). The relevance of Wnt signaling pathway to normal neural development is also well established (28). Our functional study revealed that activation of Wnt signaling in USP7-ATRT increased ZIKV^{BR}-induced tumor cell death, whereas inhibition of Wnt signaling decreased ZIKV^{BR}-induced cell death. Future alternative complementary genetic approaches should also be considered to corroborate these findings obtained with small molecules. Interestingly, an independent study using human NPC obtained from discordant dizygotic twins for congenital Zika syndrome found a similar involvement of the Wnt signaling pathway regarding differential sensitivity of NPC to ZIKV^{BR} infection (29). Translating these results to the clinical setting, patients with aggressive AT/RT and medulloblastoma should be good candidates for a future oncolytic therapy with ZIKV^{BR}, because Wnt pathway activation plays an important role in the biology of both tumor types (27, 30), contributing to stemness and therapeutic resistance (31, 32). Importantly, observed metastasis remission also suggests that a possible treatment exploring ZIKV^{BR} oncolytic effects could benefit patients with advanced and disseminated disease. Pursuit of attenuated forms of ZIKV and genetic modifications to avoid adverse effects and neutralization by the host immune system should facilitate a safe transition to clinical trials. Oncolytic viral therapy using modified Herpes simplex virus type I for melanoma has been approved by the FDA, and one clinical trial using H1-parvovirus therapy for glioblastoma is currently on phase I (33).

In conclusion, ZIKV^{BR} has strong and specific oncolytic property against human CNS embryonal tumor cells, as demonstrated by both *in vitro* and *in vivo* assays. Our results show that ZIKV^{BR} induces massive death of highly proliferative tumor cells at an MOI as low as 0.1. Selective infection of tumor cells results in low production of functional viral particles. Significant CNS tumor remission and spinal cord metastasis inhibition were also achieved after a single ZIKV^{BR} infection in tumor-bearing mice with relatively low amount of virus particles. These effects were more prominent in tumors generated by neural stem–like cancer cells with high Wnt/β-catenin basal activity. It is reasonable to speculate that other signaling pathways might contribute to tumor cell–dependent susceptibility to ZIKA-induced oncolysis, which should be further investigated. Our findings provide novel mechanistic insights and open new perspectives for future investigations using ZIKV^{BR} strains or engineered mimicking derivative approaches to treat patients affected by highly aggressive and metastatic CNS tumors lacking effective treatment.

Disclosure of Potential Conflicts of Interest

No potential conflicts of interest were disclosed.

Authors' Contributions

Conception and design: C. Kaid, E. Goulart, L.C. Caires-Júnior, K, B.H.S. Araujo, A. Telles-Silva, M. Zatz, O.K. Okamoto

Development of methodology: C. Kaid, E. Goulart, L.C. Caires-Júnior, B.H.S. Araujo, A. Soares-Schanoski, H.M.S. Bueno, K.A. Telles-Silva, R.M. Astray, M. Zatz, O.K. Okamoto

Acquisition of data (provided animals, acquired and managed patients, provided facilities, etc.): C. Kaid, E. Goulart, L.C. Caires-Júnior, A. Soares-Schanoski, H.M.S. Bueno, R.M. Astray, A.F. Assoni, A.F.R. Júnior, D.C. Ventini, A. L.P. Puglia, R.P. Gomes, M. Zatz, O.K. Okamoto

Analysis and interpretation of data (e.g., statistical analysis, biostatistics, computational analysis): C. Kaid, E. Goulart, L.C. Caires-Júnior, B.H.S. Araujo, A. Soares-Schanoski, H.M.S. Bueno, K.A. Telles-Silva, A.F. Assoni, M. Zatz, O.K. Okamoto

Writing, review, and/or revision of the manuscript: C. Kaid, E. Goulart, L.C. Caires-Júnior, B.H.S. Araujo, A. Soares-Schanoski, H.M.S. Bueno, K.A. Telles-Silva, M. Zatz, O.K. Okamoto

Administrative, technical, or material support (i.e., reporting or organizing data, constructing databases): C. Kaid, E. Goulart, L.C. Caires-Júnior, A. Soares-Schanoski, M. Zatz, O.K. Okamoto

Study supervision: C. Kaid, E. Goulart, L.C. Caires-Júnior, M. Zatz, O.K. Okamoto

Acknowledgments

The authors thank Drs. Patricia Semedo-Kuriki and Vivek Kumar for helping with cytometry assay and neuron differentiation, respectively. This study was supported by grants from FAPESP (CEPID number 2013/08028-1 and INCT to M. Zatz and O.K. Okamoto); C. Kaid is a fellow of CAPES (1379594); E. Goulart, A.F. Assoni, B.H.S. Araujo, and L.C. Caires-Júnior are fellows of FAPESP (2015/14821-1; 2016/09707-8; 2014/08049-1; 2017/16283-2).

Data and materials availability: Original data are curated and stored in the server of the Human Genome and Stem Cell Research Center (HUG-CELL). Requests for data may be sent to mayazatz@usp.br and keith.okamoto@usp.br.

The costs of publication of this article were defrayed in part by the payment of page charges. This article must therefore be hereby marked *advertisement* in accordance with 18 U.S.C. Section 1734 solely to indicate this fact.

Received October 16, 2017; revised February 2, 2018; accepted April 16, 2018; published first April 26, 2018.

References

1. Brasil P, Pereira JP, Moreira ME, Ribeiro Nogueira RM, Damasceno L, Wakimoto M, et al. Zika virus infection in pregnant women in Rio de Janeiro. N Engl J Med 2016;375, 2321–34.
2. Gabriel E, Ramani A, Karow U, Gottardo M, Natarajan K, Gooi LM, et al. Recent zika virus isolates induce premature differentiation of neural progenitors in human brain organoids. Cell Stem Cell 2017;20:397–406.e5.
3. Li H, Saucedo-Cuevas L, Regla-Nava JA, Chai G, Sheets N, Tang W, et al. Zika virus infects neural progenitors in the adult mouse brain and alters proliferation. Cell Stem Cell 2016;19:593–8.
4. Xie Z. Brain tumor stem cells. Neurochem Res 2009;34:2055–66.
5. Magee JA, Piskounova E, Morrison SJ. Cancer stem cells: impact, heterogeneity, and uncertainty. Cancer Cell 2012;21:283–96.

6. Panosyan EH, Laks DR, Masterman-Smith M, Mottahedeh J, Yong WH, Cloughesy TF, et al. Clinical outcome in pediatric glial and embryonal brain tumors correlates with in vitro multi-passageable neurosphere formation. Pediatr Blood Cancer 2010;55:644–51.
7. Kaufman HL, Kohlhapp FJ, Zloza AOncolytic viruses: a new class of immunotherapy drugs. Nat Rev Drug Discov 2015;14:642–62.
8. Silva PB, Rodini CO, Kaid C, Nakahata AM, Pereira MC, Matushita H, et al. Establishment of a novel human medulloblastoma cell line characterized by highly aggressive stem-like cells. Cytotechnology 2016;68:1545–60.
9. Rocha CR, Garcia CC, Vieira DB, Quinet A, de Andrade-Lima LC, Munford V, et al. Glutathione depletion sensitizes cisplatin- and temozolomide-resistant glioma cells in vitro and in vivo. Cell Death Dis 2014;5:e1505.
10. Studebaker AW, Hutzen B, Pierson CR, Russell SJ, Galanis E, Raffel C. Oncolytic measles virus prolongs survival in a murine model of cerebral spinal fluid-disseminated medulloblastoma. Neuro Oncol 2012;14: 459–70.
11. Zeltzer PM, Boyett JM, Finlay JL, Albright AL, Rorke LB, Milstein JM, et al. Metastasis stage, adjuvant treatment, and residual tumor are prognostic factors for medulloblastoma in children: conclusions from the Children's Cancer Group 921 randomized phase III study. J Clin Oncol 1999;17:832–45.
12. Benjamini Y, Hochberg Y. Controlling the false discovery rate: a practical and powerful approach to multiple testing. Journal of the Royal Statistical Society Series B (Methodological) 1995;57:289–300.
13. Mansuy JM, Dutertre M, Mengelle C, Fourcade C, Marchou B, Delobel P, et al. Zika virus: high infectious viral load in semen, a new sexually transmitted pathogen. Lancet Infect Dis 2016;16:405.
14. Ho DM, Shih CC, Liang ML, Tsai CY, Hsieh TH, Tsai CH, et al. Integrated genomics has identified a new AT/RT-like yet INI1-positive brain tumor subtype among primary pediatric embryonal tumors. BMC Med Genomics 2015;8:32.
15. Savidis G, McDougall WM, Meraner P, Perreira JM, Portmann JM, Trincucci G, et al. Identification of Zika virus and dengue virus dependency factors using functional genomics. Cell Rep. 2016;16:232–46.
16. Marceau C, Puschnik AS, Majzoub K, Ooi YS, Brewer SM, Fuchs G, et al. Genetic dissection of Flaviviridae host factors through genome-scale CRISPR screens. Nature 2016;535:159–63
17. Zhang R, Miner JJ, Gorman MJ, Rausch K, Ramage H, White JP, et al. A CRISPR screen defines a signal peptide processing pathway required by flaviviruses. Nature, 2016;535:164–8.
18. Zhu Z, Gorman MJ, McKenzie LD, Chai JN, Hubert CG, Prager BC, et al. Zika virus has oncolytic activity against glioblastoma stem cells. J Exp Med 2017;214:2843–57.
19. Bhatnagar J, Rabeneck DB, Martines RB, Reagan-Steiner S, Ermias Y, Estetter LB, et al. Zika virus RNA replication and persistence in brain and placental tissue. Emerg Infect Dis 2017;23:405–14.
20. Soares CN, Brasil P, Carrera RM, Sequeira P, de Filippis AB, Borges VA, et al. Fatal encephalitis associated with Zika virus infection in an adult. J Clin Virol 2016;83:63–5.
21. Peterson LR, Jamieson DJ, Honein MA. Zika Virus. N Engl J Med 2016;375:294–5.
22. Cao-Lormeau V, Blake A, Mons S, Lastere S, Roche C, Vanhomwegen J, et al. Guillain-Barré syndrome outbreak caused by ZIKA virus infection in French Polynesia. Lancet (London, England) 2016;387:1531–9.
23. Moghadas SM, Shoukat A, Espindola AL, Pereira RS, Abdirizak F, Laskowski M, et al. Asymptomatic transmission and the dynamics of zika infection. Sci Rep 2017;7:5829.
24. Upton J, Chan F. Staying alive: cell death in antiviral immunity. Mol Cell 2014;54:273–80
25. Han Z, Richer W, Fréneaux P, Chauvin C, Lucchesi C, Guillemot D, et al. The occurrence of intracranial rhabdoid tumours in mice depends on temporal control of Smarcb1 inactivation. Nat Commun 2016;7:10421.
26. Moreno N, Schmidt C, Ahlfeld J, Poschl J, Dittmar S, Pfister SM, et al. Loss of smarc proteins impairs cerebellar development. J Neurosci 2014;34: 13486–91.
27. Chakravadhanula M, Hampton CN, Chodavadia P, Ozols V, Zhou L, Catchpoole D, et al. Wnt pathway in atypical teratoid rhabdoid tumors. Neuro-Oncol 2014;17:526–35.
28. Pfister SM, Korshunov A, Kool M, Hasselblatt M, Eberhart C, Taylor MD. Molecular diagnostics of CNS embryonal tumors. Acta Neuropathol 2010;120:553–66.
29. Caires-Júnior LC, Goulart E, Melo US, Araujo BH, Alvizi L, Alvizi L, et al. Discondant congenital Zika syndrome twins show differential in vitro viral susceptibility of neural progenitor cells. Nat Comm 2018;9:475.
30. Northcott P, Buchhalter I, Morrissy A, Hovestadt V, Weischenfeldt J, Ehrenberger T, et al. The whole-genome landscape of medulloblastoma subtypes. Nature 2017;19;547:311–7.
31. McCord M, Mukouyama Y, Gilbert MR, Jackson S. Targeting WNT signaling for multifaceted glioblastoma therapy. Front Cell Neurosci 2017;13;318.
32. Cho YJ, Tsherniak A, Tamayo P, Santagata S, Ligon A, Greulich H, et al. Integrative genomic analysis of medulloblastoma identifies a molecular subgroup that drives poor clinical outcome. J Clin Oncol 2011;10: 1424–30.
33. Lawler SE, Speranza MC, Cho CF, Chiocca EA. Oncolytic viruses in cancer treatment. JAMA Oncol 2017;3:841.